Available online at www.sciencedirect.com
SCIENCE DIRECT®
Journal of Power Sources 141 (2005) 163–166
JOURNAL OF POWER SOURCES
www.elsevier.com/locate/jpowsour

Enhancement of capacity and cycle-life of $Sn_{4+\delta}P_3$ ($0 \leq \delta \leq 1$) anode for lithium secondary batteries

Young-Ugk Kim[a], Sung-Il Lee[a], Churl Kyung Lee[b], Hun-Joon Sohn[a,*]

[a] *School of Materials Science and Engineering, Research Center for Energy Conversion and Storage, Seoul National University, Seoul 151-742, South Korea*
[b] *School of Materials and System Engineering, Kumoh National Institute of Technology, Kumi, Kyungbuk 730-701, South Korea*

Received 16 May 2004; accepted 2 September 2004
Available online 19 November 2004

Abstract

Various compositions of tin-rich, non-stoichiometric, solid solutions of $Sn_{4+\delta}P_3$ are synthesized by a mechanochemical method. The materials are tested as anodes for lithium secondary batteries to enhance reversible capacity and cycleability. Investigative analyses show that the region for the solid-solution formation of $Sn_{4+\delta}P_3$ is $0 \leq \delta \leq 1$. The reaction mechanism of the tin-rich solid solutions is similar to that of stoichiometric Sn_4P_3, except for the absence of a topotactic lithium insertion reaction during the first cycle. As the tin content is increased, tin-rich phosphide exhibits better cycleability and retains a higher reversible capacity, namely, about 20% more than that of stoichiometric Sn_4P_3.

Keywords: Tin phosphide; Anode; Capacity; Solid solution; Cycle performance; Lithium battery

1. Introduction

At the present time, carbon–lithium compounds are the most commonly used anode materials in commercial secondary lithium batteries. They offer a good compromise for different requirements, but their specific capacity is rather low (372 mAh g^{-1} for graphite). Recently, higher capacity alternatives to carbon-based anode materials are being actively pursued. Among the candidates, tin-based composites exhibit higher capacities than those of carbonaceous materials, but have poor cycleability due to large volume changes during cycling. Nanocrystallization of active materials with an inactive matrix such as tin-based composite oxides have been investigated in attempts to improve poor cycleability [1–6].

Four forms of tin phosphides are available [7,8], viz., SnP_3, Sn_3P, SnP, and Sn_4P_3. In our previous studies [9,10], the reaction mechanism and electrochemical performance of Sn_4P_3 as an anode material have been investigated. This stoichiometric tin phosphide retains a reversible capacity of 370 mAh g^{-1} up to 50 cycles when cycled within a limited voltage window where Li_3P is stable. On the other hand, it suffers from a relatively large irreversible capacity due to the formation of Li_3P during the first cycle and Sn_4P_3 still contains a high phosphorous content. To improve the initial cyclic efficiency and to increase the reversible capacity, an attempt was made to increase the tin content in Sn_4P_3 active material by solid-solution formation while sustaining the reaction mechanism of Sn_4P_3. The mechanical alloying technique, which is known to be a very effective method for the extension of the solid solubility [11], was employed to prepare the tin-rich solid solution. In this study, the solid solubility limit of Sn in $Sn_{4+\delta}P_3$ via mechanical alloying has been determined and the electrochemical properties of the tin-rich solid solutions have been investigated.

2. Experimental

Active materials were prepared by using Sn (>99%, Aldrich) and red phosphorous (>99%, Aldrich) powders as precursors for mechanochemical synthesis. Various ratios of

* Corresponding author. Tel.: +82 2 880 7226; fax: +82 2 885 9671.
E-mail address: hjsohn@snu.ac.kr (H.-J. Sohn).

0378-7753/$ – see front matter © 2004 Published by Elsevier B.V.
doi:10.1016/j.jpowsour.2004.09.007

the precursor powders were placed in a hardened steel vial with hardened steel balls at a ball-to-powder ratio of 20 to 1. The vial was assembled in an argon-filled glove-box, and then mounted on a SPEX-8000 vibratory mill. Each sample was characterized by X-ray diffraction (XRD) analysis using a MacScience MXP18A-SRA diffractometer.

The test electrodes consisted of the powdered active material, denka black as a conducting agent, and polyvinylidene fluoride (PVdF) dissolved in *N*-methyl pyrrolidinon (NMP) as a binder, with a mass ratio of 8:1:1. Each component was well mixed to form slurry, which was coated on a copper foil and then pressed and dried at 120 °C for 4 h under vacuum. A laboratory-made, coin type, electrochemical cell was used with lithium foil as a counter electrode and 1 M $LiPF_6$ in a mixed solvent of ethylene carbonate and diethylene carbonate (EC + DEC, 1:1, v/v, Cheil industry) as an electrolyte. Cell assembly and all electrochemical tests were conducted in an argon-filled glove-box. Charge (Li insertion)–discharge (Li removal) experiments were performed galvanostatically at a current density of 100 mA g^{-1}. To confirm the formation of a tin-rich solid solution, scanning tunnelling electron microscopic (STEM) (JSM-3000F, JEOL) and scanning Auger microprobe (SAM) (Model 660, Perkin-Elmer) analyses were performed.

3. Results and discussion

The X-ray diffraction patterns of active materials synthesized by mechanical alloying with various Sn:P ratios are shown in Fig. 1. All the peaks can be completely indexed as the stoichiometric Sn_4P_3 phase based on the hexagonal crystal system of $R\bar{3}m$ [12]. No other minor and/or impurity phases are observed. Nevertheless, the Bragg peak shifts towards a lower angle on increasing the tin content in the compound, as shown in the insert of Fig. 1. Lattice parameters have been calculated from the peak shift as a function of excess tin content (δ) using a Si internal standard method, and are presented in Fig. 2. The lattice parameter increases linearly up to $\delta = 1$, and hence satisfies Vegard's law [13]. This

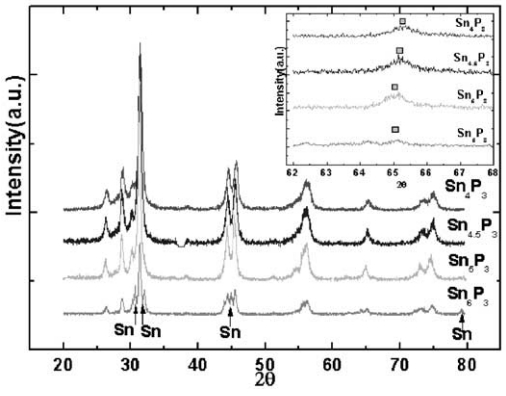

Fig. 1. X-ray diffraction patterns of active materials with various Sn:P ratios.

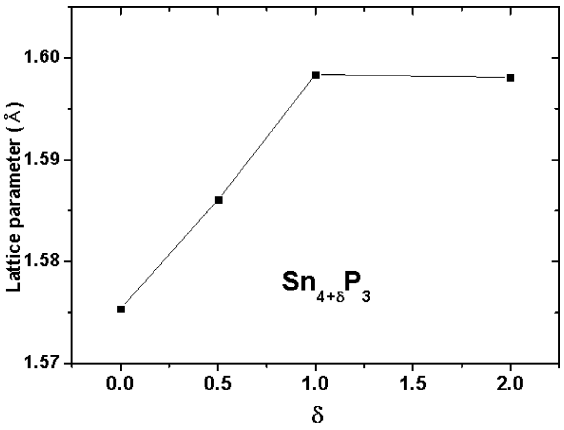

Fig. 2. Lattice parameters calculated from XRD peak shift as function of excess tin content.

is a typical feature of a solid solution. The lattice parameter of Sn_6P_3 is almost the same as that of Sn_5P_3, but a metallic tin phase appears in the XRD pattern, as shown in Fig. 1. Thus, it is concluded that excess tin beyond $\delta = 1$ remains as a metallic phase, and that the limit of solid-solution formation is approximately Sn_5P_3.

The absence of solute peaks in the XRD patterns is usually taken as a proof of complete dissolution, and this has been interpreted as evidence for enhanced solid solubility limits. It has been shown recently that the solid solubility limits cannot be accurately determined by absence of solute peaks in the XRD patterns. In the Al–20 wt.% Ti system, Kim et al. [14] observed that the Ti reflections were absent in the XRD pattern. Nevertheless, tunnelling electron microscope investigations of the same powder clearly demonstrated the presence of Ti particles in the aluminum matrix. This suggested that the absence of XRD peaks from the solute phase might not be sufficient evidence for complete solid solubility. To confirm solid solution formation, element mapping using a scanning tunnelling electron microscope was carried out; the results are presented in Fig. 3. Both tin and phosphorous are found to be homogeneously dispersed, which is the general feature of solid solution states, and no traces of condensed tin and/or phosphorous regions are observed. To obtain statistical data of elemental dispersion, scanning Auger microprobe analyses were conducted using Sn_4P_3 as a reference material. Data were collected at three points of each sample and then averaged. The relative ratios of tin to phosphorous are presented in Table 1, and the synthesized materials are found to be chemically homogeneous throughout the sample (within instrumental error), which is in good agreement with XRD and STEM results.

Table 1
Elemental analysis by scanning Auger microprobe corrected with Sn_4P_3 reference

	x in Sn_xP_3
Sn_4P_3	4 (reference)
$Sn_{4.5}P_3$	4.522
Sn_5P_3	4.998

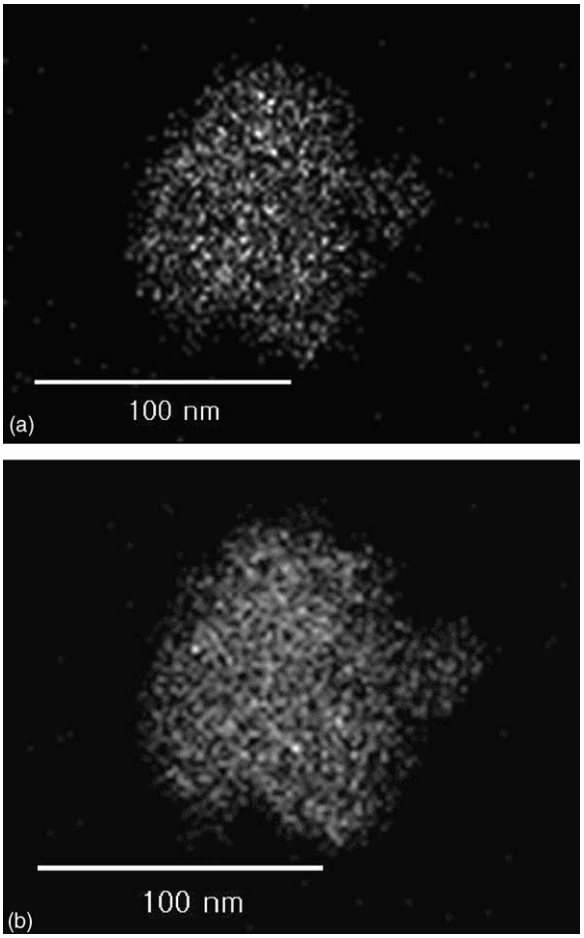

Fig. 3. (a) Element mapping of phosphorous using a scanning tunnelling electron microscope. (b) Element mapping of tin using a scanning tunnelling electron microscope.

Initial voltage profiles of Sn_4P_3, $Sn_{4.5}P_3$, and Sn_5P_3 charged–discharged at a rate of 100 mA g^{-1} are demonstrated in Fig. 4. During the first discharge, the capacities slightly decrease as the relative content of phosphorous,

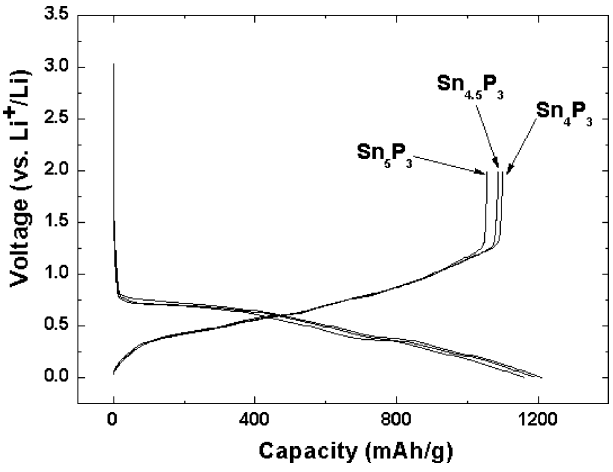

Fig. 4. Initial voltage profiles of Sn_4P_3, $Sn_{4.5}P_3$, and Sn_5P_3.

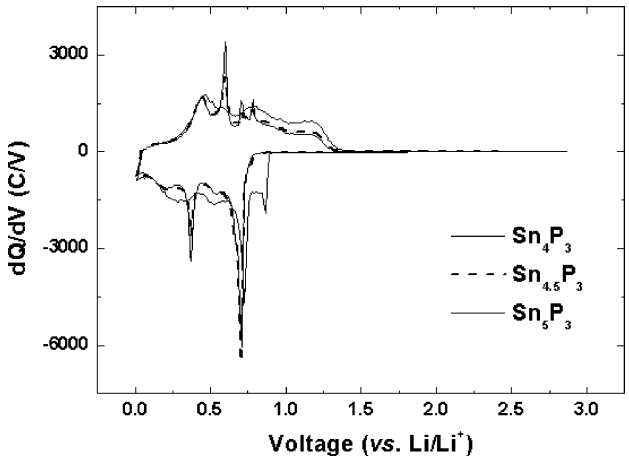

Fig. 5. Differential capacity plots of Sn_4P_3, $Sn_{4.5}P_3$, and Sn_5P_3.

which is able to uptake more lithium than tin, decreases. The profiles look smooth over the voltage range, except for short voltage plateaux at around 0.72 and 0.40 V. On the first charge, the shape is also smooth, which is a typical feature for active material with a low crystallinity. The first discharge and charge capacities of these materials are much larger than those of commercialized carbonaceous materials and initial cyclic efficiencies are above 90%.

Differential capacity plots of Sn_4P_3, $Sn_{4.5}P_3$ and Sn_5P_3 are presented in Fig. 5. Cells were galvanostatically charged and discharged at a current density of 100 mA g^{-1}. In our previous report [10], we suggested a three-step reaction mechanism for Sn_4P_3, as follows: (i) insertion of Li into the layered structure of Sn_4P_3; (ii) formation of various phases of Li_xP approximately between 0.8 and 0.6 V; (iii) formation of Li_xSn alloy and Li_3P below 0.6 V.

Unlike Sn_4P_3, the reaction peak at 0.86 V, which is assigned to the topotactic lithium insertion reaction, is absent in the differential capacity plots of $Sn_{4.5}P_3$ and Sn_5P_3. This is probably due to fact that the tin atoms, which are inserted excessively into the stoichiometric hexagonal layer structured Sn_4P_3, hinder the insertion reaction so that lithium cannot react with the active material until the Sn–P bonds are broken at 0.72 V, and the sequential reaction steps are identical to those of Sn_4P_3, as suggested above. As shown in Fig. 5, the reaction peaks that correspond to Sn–Li alloying become larger as the tin content increases.

The cycle performance of Sn_4P_3, $Sn_{4.5}P_3$, and Sn_5P_3 electrodes are compared in Fig. 6. Between 0.0 and 1.4 V, the electrodes show a drastic decline in capacity which is due to the irreversibility of LiP phase that is formed and the agglomeration of tin atoms [15,16]. If the potential window is limited between 0.0 and 0.72 V, where the Li_3P matrix is stable with no agglomeration of tin atoms, the electrodes display an enhanced cycle performance. As mentioned previously, the initial discharge capacity of Sn_4P_3 is slightly larger than that of Sn_5P_3, while the initial charge capacity of the latter is larger than that of the former by about 20% throughout the

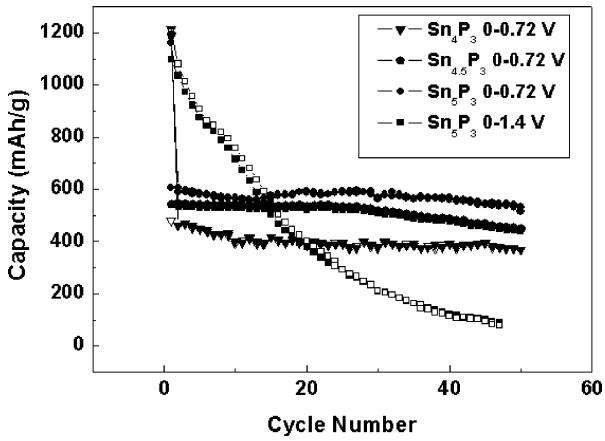

Fig. 6. Cycle performances of Sn_4P_3, $Sn_{4.5}P_3$, and Sn_5P_3.

test, which is in a good agreement with the tin content of these electrodes. The Sn_5P_3 electrode exhibits a relatively good capacity retention of above 530 mAh g^{-1} even after 50 cycles compared with the stoichiometric Sn_4P_3, viz., 370 mAh g^{-1} at the 50th cycle.

4. Conclusions

Tin-rich solid solutions of Sn_4P_3, $Sn_{4+\delta}P_3$ ($0 \leq \delta \leq 1$), have been synthesized by means of a mechanochemical route. As the tin content is increased, the lattice parameter increases linearly until up to Sn_5P_3, which is a typical feature of solid-solution formation. To confirm solid-solution formation, complementary analyses such as STEM and SAM analyses have also been performed. Unlike Sn_4P_3, topotactic lithium insertion is not observed for $Sn_{4.5}P_3$ or Sn_5P_3. This is probably due to a hindrance effect of excess tin atoms, though the sequential reactions are identical to that of Sn_4P_3. Due to the large content of tin formed from decomposition of the active material and the Li_3P matrix, Sn_5P_3 displays a larger reversible capacity than that of Sn_4P_3, as well as a relatively good performance up to 50 cycles with capacity above 530 mAh g^{-1} for a limited voltage window. From these results, it is concluded that the formation of active material with a tin-rich solid solution provides a means to improve the performance of anode materials in secondary lithium batteries.

Acknowledgements

The authors are grateful for financial support from KOSEF through the Research Center for Energy Conversion and Storage at Seoul National University.

References

[1] Y. Idota, T. Kubota, A. Matsufuji, Y. Maekawa, T. Miyasaka, Science 276 (1996) 1395.
[2] J.O. Besenhard, J. Yang, M. Winter, J. Power Sources 68 (1997) 87.
[3] K.D. Kepler, J.T. Vaughey, M. Thackeray, Electrochem. Solid-State Lett. 2 (1999) 307.
[4] H. Kim, B. Park, H.-J. Sohn, T. Kang, J. Power Sources 90 (2000) 59.
[5] I.A. Courtney, J.R. Dahn, J. Electrochem. Soc. 144 (1997) 2045.
[6] D.G. Kim, H. Kim, H-J. Sohn, T. Kang, J. Power Sources 104 (2002) 221.
[7] T.B. Massalski, Binary Alloy Phase Diagram, vol. 2, first ed., American Society for Metals, 1989, p. 1828.
[8] JCPDS, file no. 42-1051.
[9] Y.-U. Kim, D.G. Kim, H.-J. Sohn, T. Kang, no. 33, Abstract, 11th IMLB, Monterey, USA (2002).
[10] Y.-U. Kim, C.-K. Lee, H.-J. Sohn, T. Kang, J. Electrochem. Soc. 151 (2004) A933.
[11] G. Suryanarayana, Prog. Mater. Sci. 46 (2001) 1.
[12] JCPDS, file no. 20-1294.
[13] L. Vegard, Z. Phys. 17 (1921) 5.
[14] H.-S. Kim, D.-S. Suhr, G.-H. Kim, D.-W. Kum, Met. Mater. Int. 2 (1996) 15.
[15] I.A. Courtney, J.R. Dahn, J. Electrochem. Soc. 144 (1997) 2045.
[16] J.H. Kim, G.-J. Jeong, Y.-W. Kim, H.-J. Sohn, C.W. Park, C.K. Lee, J. Electrochem. Soc. 150 (2003) A1544.